ChemPhysChem

Research Article
doi.org/10.1002/cphc.202200723

Chemistry Europe
European Chemical Societies Publishing

www.chemphyschem.org

Ethanol Oxidation Reaction Mechanism on Gold Nanowires from Density Functional Theory

O. V. M. Bueno,[a] M. A. San-Miguel,[b] and E. Z. da Silva*[a]

Thin gold nanowires (NWs) are materials that could be used as support in different chemical reactions. Using density functional theory (DFT) it was shown that NWs that form linear atomic chains (LACs) are suitable for stimulating chemical reactions. To this end, the oxidation reaction of ethanol supported on the LACs of Au–NWs was investigated. Two types of LACs were used for the study, one pure and the other with an oxygen impurity. The results showed that the oxygen atom in the LAC fulfills important functions throughout the reaction pathway. Before the chemical reaction, it was observed that the LAC with impurity gains structural stability, that is, the oxygen acts as an anchor for the gold atoms in the LAC. In addition, the LAC was shown to be sensitive to disturbances in its vicinity, which modifies its nucleophilic character. During the chemical reaction, the oxidation of ethanol occurs through two different reaction paths and in two stages, both producing acetaldehyde (CH_3CHO). The different reaction pathways are a consequence of the presence of oxygen in the LAC (oxygen conditions the formation of reaction intermediates). In addition, the oxygen in the LAC also modifies the kinetic behavior in both reaction stages. It was observed that, by introducing an oxygen impurity in the LAC, the activation energy barriers decrease ~69% and ~97% in the first and second reaction stages, respectively.

Introduction

Gold, a noble metal, is a very stable and nonreactive material in its bulk form. With the advent of new experimental tools such as high-resolution electron microscopy (HREM), atomic force microscopy (AFM), and scanning tunneling microscopy (STM), for manipulating atoms and high-resolution imaging; various types of gold nanostructures have been studied, such as nanoclusters and nanowires.[1–6] At the beginning of the XXI century, gold nanostructure studies were able to experimentally produce very thin nanowires, as thin as a one-dimensional linear atomic chain (LAC) with four to ten gold atoms.[7–11] These studies revealed many interesting properties, some of which are their structures and reactivity. One of its most studied properties was their structures, specifically, the unusually large Au–Au bond distances of ~3.6 Å.[10] These intriguing results sparked many experimental and theoretical works.[7,8,10–15] The first computational studies of pure gold NWs failed to reproduce the large distances observed experimentally. On the other hand, HRTEM experiments suggested the possible contamination of the NWs with light atoms that could be the culprits for the observed results.[10,13,14] Subsequently, theoretical works using computer simulations studied the effect of impurities in an attempt to explain the experimental results. H, C, O, among other contaminants, were considered.[13–15] The reasoning was that although experiments were in high vacuum, there is always a possibility that some residual molecules, such as O_2, CO, CO_2, or H_2O, could contaminate the NWs. Theoretical studies, in the first instance, considered H as the probable contaminant.[14] Further research showed that O could also be a contaminant, with interesting mechanical effects on the Au–NWs, where Au–O–Au bonds helped the formation of longer LACs.[15] Further experimental work verified the theoretical predictions of the large distances associated with H and O contaminants.[8]

The mechanism that explained the incorporation of O in the LAC through a chemical reaction between O_2 and CO molecules in Au–NW showed that O_2 and CO could form an intermediate (–Au–COO_2–Au–), which under stress could evolve to the production of a CO_2 molecule released into the gas phase, leaving an atomic oxygen impurity in the LAC (–Au–O–Au–).[16] The behavior of Au–NWs suggests that the LACs are reactivate. This would open up new opportunities and NWs can possibly be used to stimulate various types of chemical reactions, similar to how previously shown with gold nanoclusters.[17–21] It should be noted that NWs could be materials with limited use. Its complex structure could be a limiting factor both in its manufacture and in its sustainability and/or stability over time. However, this problem could be overcome by designing systems that constantly produce NWs, that is, systems that allow them to be obtained at every instant of time. Mechanically controllable break-junction method[22] allows this characteristic, therefore, NWs would be manufactured constantly, thereby eliminating the issue of stability and sustainability. In addition, it is necessary to take into account that NWs, being relatively new materials, its manufacture occurs at the laboratory scale. Therefore, NWs could be considered possible materials with great potential for catalytic use.

[a] Dr. O. V. M. Bueno, Prof. E. Z. da Silva
Institute of Physics 'Gleb Wataghin'
University of Campinas-Unicamp
13083-859 Campinas, SP, Brazil
E-mail: zacarias@ifi.unicamp.br
[b] Prof. M. A. San-Miguel
Department of Physical Chemistry, Institute of Chemistry
University of Campinas-Unicamp
P. O. Box 6154, 13083-970 Campinas, SP, Brazil

Supporting information for this article is available on the WWW under https://doi.org/10.1002/cphc.202200723

Considering the reactive capacity of Au–NWs with LACs and following the reactivity studies in Au–NWs,[16] in this work, we continue to explore the reactivity of Au–NWs. For this, the LAC was defined considering its pure form (four Au atoms, Figure 1) and with impurity (four Au atoms and one oxygen atom, Figure 1). The reaction mechanisms of ethanol oxidation supported in Au–NW are investigated, with new and interesting results. We chose ethanol with the intention of also exploring the activation of the C–H bond in the $-CH_2-$ group. The activation of the C–H bond is well established in the literature and is defined as the β-C–H mechanism[23–26] and in this work we explore the mechanism of breaking the C–H bond of ethanol.

Methodology

The present work employed the program package CP2K,[27,28] where the module QUICKSTEP[29] was used to combine gaussians and plane waves (GPW).[30] Wave functions were expanded in plane waves and gaussians, with a 650 Ry cutoff for plane waves and multiple grid mapping with a real cutoff of 80 Ry. The orbital transformation method[31] was used for efficient wave function optimization. The electronic structure was calculated with density functional theory (DFT) using the Perdew-Burke-Ernzerhof (PBE) functional[32,33] together with the reparameterization of an empirical analytical potential of Grimme's D3 dispersion correction[34–36] in the range of 15 Å. For all atoms except Au, the TZV2P-MOLOPT-GTH basis set was used. For Au atoms, the DZVP-MOLOPT-SR-GTH basis set was used.[37] Geodecker-Teter-Hutter (GTH) relativistic pseudopotentials were adopted to model the core electron.[38,39] Valence electrons for Au = 5d106s, O = 2s22p4 and C = 2s22p2 were used. Additionally, we use different methodologies, in a particular chemical reaction, to show the consistency of our methodology. For them, we choose the functionals B3LYP/D3BJ[40,41] and ωB97X/D3[42,43] using the basis sets def2-TZVP for the C, H, O atoms and LANL2TZ(f)[44–46] for the Au atoms. Details are in the supplementary material (Figure S2).

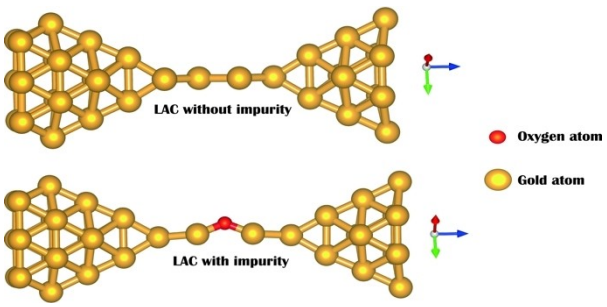

Figure 1. Au–NW (theoretical models) considered in our simulations. LAC with four Au atoms (top image) and LAC with four Au atoms and one oxygen impurity (bottom image). These structures were taken from references[15,16] and later relaxed and optimized. For more details on the optimization methodology used, see supplementary material (Figure S1).

In the DFT-based *ab initio* molecular dynamics simulations, the timestep was set to 0.5 fs for all our simulations. The simulation temperature was adjusted to 300 K (NVT statistical ensemble) using Nosé-Hoover chain thermostats.[47–49] Equilibration process was performed using a massive Nosé-Hoover chain thermostat, with the thermostat-time-constant set to $\tau = 10$ fs. Subsequently, each system was simulated for 2ps with a global Nosé-Hoover chain thermostat (thermostat-time-constant $\tau =$ 50 fs) before starting production. The simulation cell sizes in XY were chosen so that an empty space between the nanowires was guaranteed, avoiding the interaction between periodic images ($x = y = 20$ Å). The simulation trajectories showed that the ethanol molecule moves around the gold nanowire, staying infrequently in the vicinity of the LAC, exploring a large number of configurations of little interest for our purpose. Taking this into account, the movement of ethanol was constrained to the vicinity of LAC using an upper harmonic wall with a spring constant of $k = 200$ kcal mol^{-1} Å^{-2}.

To find chemical reactions of interest with a short simulation time, the molecular dynamics were accelerated using two techniques: (i) metadynamics[50] and (ii) the extended Lagrangian metadynamics scheme,[51] all implemented in the program package CP2K.[27,28] In both techniques, reaction coordinates (collective variables) were defined using distances between atoms. In the *ab initio* dynamics simulations, using metadynamics, gaussians were added every 30 fs. The height of the gaussians was defined as 4.5 kcal/mol and the width of the gaussians was defined as 0.9 Å. The parameters within the Lagrangian formalism were defined with a virtual particle mass of 30.0 a.m.u., a coupling spring constant $\lambda = 2.0$ (lambda), and the temperature of the auxiliary variables at 300 K.

The minimum energy path of all chemical reactions was quantified using the harmonic nudged elastic band (NEB) method. Specifically, the climbing-image nudged elastic band (CI-NEB)[52,53] was used. The spring constant value for NEB calculations was set to 0.02 au. In some cases, the minimum energy path has been quantified using free energy surfaces[54] using well-tempered metadynamics. The additional parameter that requires well-tempered metadynamics (polarization temperature) was set to 15000 K. This value proved to be adequate to overcome energy barriers of approximately 30.0 kcal mol^{-1}.

Results and Discussion

Topological Analysis of Au–NW LAC

Previous work has shown that O2 and CO molecules can react with LAC to form Au–O–Au bonds.[16] Au–O bonds seem to be stronger than pure Au–Au bonds, favoring the stability of NWs that were contaminated with oxygen impurities.[15] To further verify this point, using electron location function (ELF), we analyze the chemical bond between Au–Au and Au–O atoms. See supplementary material (Figure S3) for technical details.

Pure LAC displays regions of highly localized electron density around the nuclear centers that suffer distortions due to their structural arrangement (Figure 2A, red color), which leads

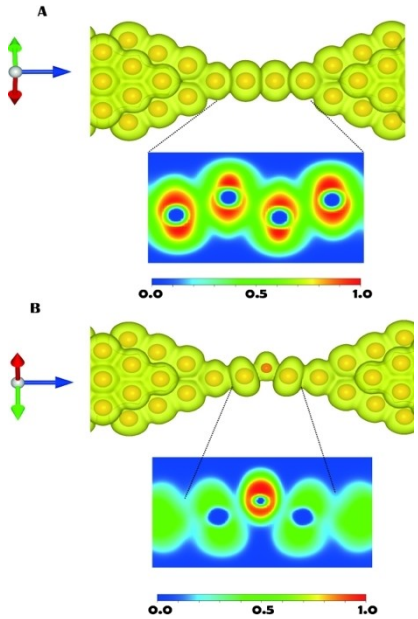

Figure 2. Analysis of the electron location function (ELF) isosurfaces for the gold nanowire without and with the presence of the impurity. (A and B) representation of the 3D ELF with n = 0.157 and the 2D ELF planes of the linear atomic chain (LAC).

to the loss of their spherical distribution, as observed in their bulk form. The LAC with one impurity drastically loses its highly localized electron density along the linear chain (Figure 2B). This can be attributed to the high electronegativity of oxygen, which modifies the electron density localization of all gold atoms of the LAC. This shows that the Au nanowire, specifically within the LAC, could show different chemical behavior, both without and with the presence of impurity. Therefore, the chemical reactions that could take place would be given by different reaction paths, or at least have a different kinetic behavior.

Using the ELF 1D profile between neighboring Au–Au regions, characteristic $\eta(r)$ values of a metallic bond[55] can be observed (Figure S3, profile 1 and profile 4). Furthermore, it is observed that the $\eta(r)$ ELF profile corresponding to the Au–O bond starts with a typical behavior of a covalent bond ($\eta(r) \approx 0.8$), which decreases to a typical value of a metallic bond ($\eta(r) \approx 0.26$), with the presence of a characteristic local minimum (Figure S3, profile 2 and profile 3). To analyze the stability window for the Au–O bond, the localization window concept was used (difference between a nonnuclear maximum ELF value and the first order saddle point).[55,56] It is observed that a value of $\eta(r) \approx 0.07$ makes clear that the Au–O bond is much stronger than a neighboring Au–Au bond, which has a value of $\eta(r) \sim 0.1$. In an alternative way, this can also be checked by determining the difference in bond energy between Au–Au and Au–O, in the LAC. Defining an ideal reaction of the type: tip≡Au–Au–O–Au≡tip + Au → tip≡Au–Au–Au–Au≡tip + O, it is obtained that $\Delta E = 0.59$ eV, consult supplementary material. Therefore, these results show that the impurity (oxygen) in the LAC fulfills two important functions: (i) it modifies the chemical nature of the LAC, which could lead to different chemical reactions, and (ii) it stabilizes the LAC by acting as an anchor between gold atoms.

Active Sites in Au–NW LAC

The active chemical sites in Au–NWs were qualitatively explored using the molecular electrostatic potential (MEP) mapping function.[57] MEP analysis is most useful when representing color-coded electronic density and represented on equipotential surfaces (Figure 3). The surface analysis allows visualization of regions of a molecule with variable charge showing them as surfaces with excess and deficiency of electrons.[58] The first row (Figure 3, structures A1–A4) shows the LAC without impurity, where different perspectives of the LAC view can be observed. Similarly, the second row presents the LAC with an oxygen

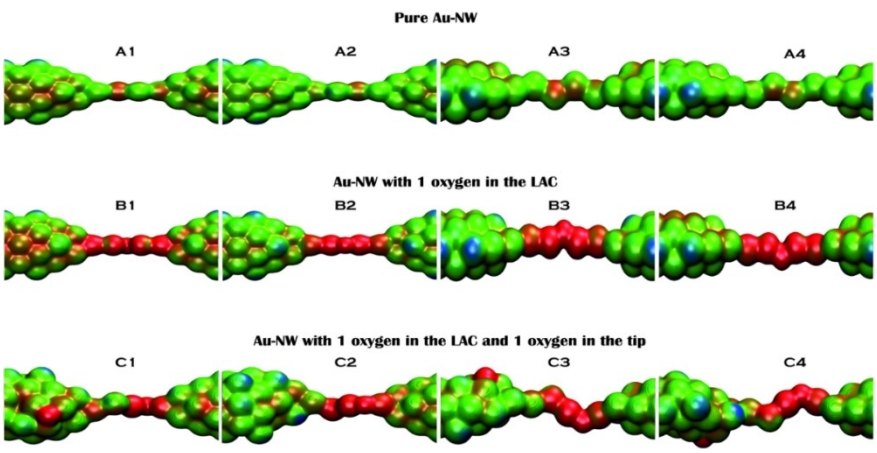

Figure 3. The images show the molecular electrostatic potential (MEP) map projected onto a surface of isodensity defined at 0.001 electrons/bohr3. A1–A4 show the LAC without the presence of oxygen in its structure. B1–B4 show LAC with an oxygen atom in its structure. C1–C4 show the LAC with an oxygen atom in its structure and an oxygen atom at the tip of its structure. Deficiency and excess load are represented by blue and red colors, respectively. The color scale was defined in BGR format in the range of −0.007 to 0.09.

impurity (Figure 3, structures B1–B4), and the third row shows an oxygen impurity in the LAC and an oxygen impurity at the tip (Figure 3, structures C1–C4).

It is observed that Au–NW without oxygen impurity in its structure maintains approximately charge neutrality (green) across its surface, with a slight displacement of positive (blue) and negative (red) charges (Figure 3, where A1–A4 show different viewing perspectives of the pure NW). This behavior suggests that Au–NW could have a weak nucleophilic and/or electrophilic character. Accordingly, possible chemical reactions with organic molecules, such as ethanol, could occur with difficulty. However, when introducing an oxygen impurity into the LAC (Figure 3, where B1–B4 show different perspective views of the NW with an oxygen atom in the LAC), the gold atoms acquire a partial negative charge (red). This behavior makes the LAC increase its nucleophilic character, that is, becoming an active site to stimulate the chemical reaction. Additionally, when an oxygen impurity is introduced at the tip of the Au–NW, no charge distribution is observed (Figure 3, where C1–C4 show different view perspectives of the NW with an oxygen atom in the LAC and an oxygen atom in the tip); that is, the gold atoms maintain their initial charge neutrality (green).

All these results suggest that the most sensitive active site of Au–NW is specifically in LAC, and consequently, the nanowire tip is of little interest in comparison with the LAC. Therefore, it can be said that the presence of the oxygen impurity in the LAC of the Au–NW specifically modifies its nucleophilic character. This apparently special feature of LAC has been observed in other studies,[59,60] showing to be a common behavior. In these, it was also observed that the transition metal LACs could easily create centers with excess and deficient charge. Therefore, considering these results, our reactivity study will be restricted to LAC.

Interaction of Ethanol with LAC

The charge redistribution in the interaction of ethanol with Au–NWs was analyzed with the electron density difference (EDD). To know the technical details of how the EDD was defined, consult supplementary material. In the study, two situations were defined: (i) the interaction of ethanol with the pure LAC and (ii) the interaction of ethanol with the LAC containing an oxygen impurity. (Figure 4). In the pure LAC, charge redistribution occurs mainly through the interaction between H (–O**H** group) and LAC atoms, and to a lesser extent between O (–**O**H group) and LAC atoms (Figure 4, A1–A2), observing in these cases the flow of charge toward the LAC. Similarly, in the LAC with an oxygen impurity, charge redistribution towards the LAC occurs mainly through the interaction between the O and LAC atoms (Figure 4, B1–B2). This shows that ethanol also contributes to the increase in the nucleophilic character of LAC, both in pure LAC and in LAC with an oxygen impurity. Therefore, the presence of ethanol near the LAC plays an important role before any chemical reaction even occurs. In addition, it is suggested that in a more realistic system, that is, a system with a higher ethanol concentration, the amount of ethanol could play an important role, such as defining the nucleophilic character of Au–NW. These results show that the LAC is sensitive to disturbances in its environment, making NWs an optimal material to stimulate chemical reactions.

Additionally, adsorption energy[61] calculations (see supplementary material for technical details) showed that the adsorption of ethanol in the LACs without and with impurity presented adsorption energies of −0.638 eV and −0.958 eV, respectively. The magnitude of these energies is consistent for similar systems, such as ethanol absorbed on the surface of platinum.[111][62] Considering the thermal fluctuation of our system at 300 K, which is equivalent to fluctuations of the order of ~0.0259 eV, we can suggest that, in a possible chemical reaction between ethanol on the LAC, the ethanol-LAC adsorption energy plays an important role in the initiation of the reaction kinetics.

Ethanol Oxidation Reaction Mechanisms

Ethanol oxidation reactions were studied with *ab initio* molecular dynamics in conjunction with well-tempered metadynamics

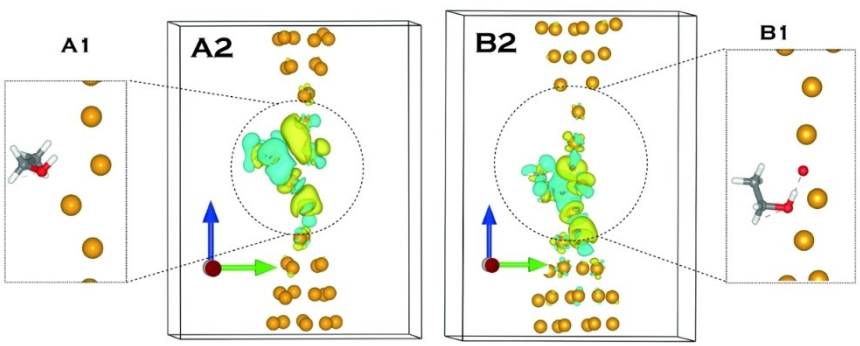

Figure 4. Electron density difference (EDD) defined to study the charge rearrangement caused by the presence of ethanol. (A1 and B1) represent the nanowire without and with the presence of impurities. (A2 and B2) represent the differences in charge density ($\Delta\varrho$) of the nanowires/ethanol defined in A1 and B1. The light yellow and light green regions indicate electron accumulation and depletion, respectively.

to observe chemical reactions with shorter simulation times. As suggested by the MEP, EDD, and ELF studies, the ethanol molecule was conveniently restricted to the vicinity of LAC to take advantage of its reactivity potential. It also helped to reduce the computational cost, avoiding exploring regions irrelevant to our purpose.

The thermodynamic stability at room temperature of our system (NW) was confirmed by calculating the Gibbs free energy of the system. For them the linear atomic chain length of the NW was used as a collective variable (Supplementary Material, Figure S4). The results showed that NWs are indeed stable at room temperature. Confirmed the thermodynamic stability of our system, we start our reactivity study.

Pristine Au LAC

The free-energy landscape of the interaction between the ethanol molecule and Au–NW LAC was constructed using the reaction coordinates CV1 = d(OH–Au) and CV2 = d(CH2–Au) as collective variables (Figure S5). It is observed that, at room temperature (300 K), ethanol through its three functional groups (–CH_3, –CH_2–, and –OH) interacts very frequently with the LAC, defining three different local minima, where Au–CH_3, Au–CH_2, and Au–OH interactions prevail over time (Figure S5 B–D, blue color). The three preferred conformations adopted by ethanol in LAC suggest that the chemical reaction could occur with any of the groups –CH_3, –CH_2– and –OH. Therefore, to explore these possible reactions, surface potential energy scans were performed. For this, the distances defined by the atoms **C**H_3–**Au** (Figure S6A), **C**H_2–**Au** (Figure S6B), and **O**H–**Au** (Figure S6C) were used. It is observed that of the three groups analyzed (Figure S6A, B, and C), the –CH_2– group when approaching the gold atom at ~2.3 Å presents an abrupt energy drop (Figure S6B). The drop in energy is related to the transfer of one of the hydrogens from the –CH_2– group to the LAC (Figure S6B, observe B2–B3 distances). Furthermore, the –CH_2– group turns out to be the only one that favors a chemical reaction with lower energy cost. That is, the activation of the β-C–H bond of the –CH_2– group is observed, involving the formation of acetaldehyde as a reaction product.[63] Considering this result, the reaction coordinate, that is, the d(CH_2–Au) distance, was chosen to be used as a collective variable in the simulation of *ab initio* molecular dynamics with metadynamics.

The study starts by stimulating the chemical reaction for the pure LAC (Figure 5A). Metadynamics was applied only until the chemical reaction occurred (Figure 5B). It is observed in this process that the potential energy of the system fluctuates abruptly (during the use of metadynamics) due to the formation and breaking of chemical bonds. The trajectory analysis shows that the chemical reaction occurs with the formation of an intermediary in its first step (Figure 5A). The time evolution of the Au–C distance (Figure 5C) shows that the intermediate begins to form when the Au–C distance acquires values less than 5.0 Å. Once the intermediary was formed, another molecular dynamics routine simulation (without metadynamics) was performed to further analyze the stability of the interme-

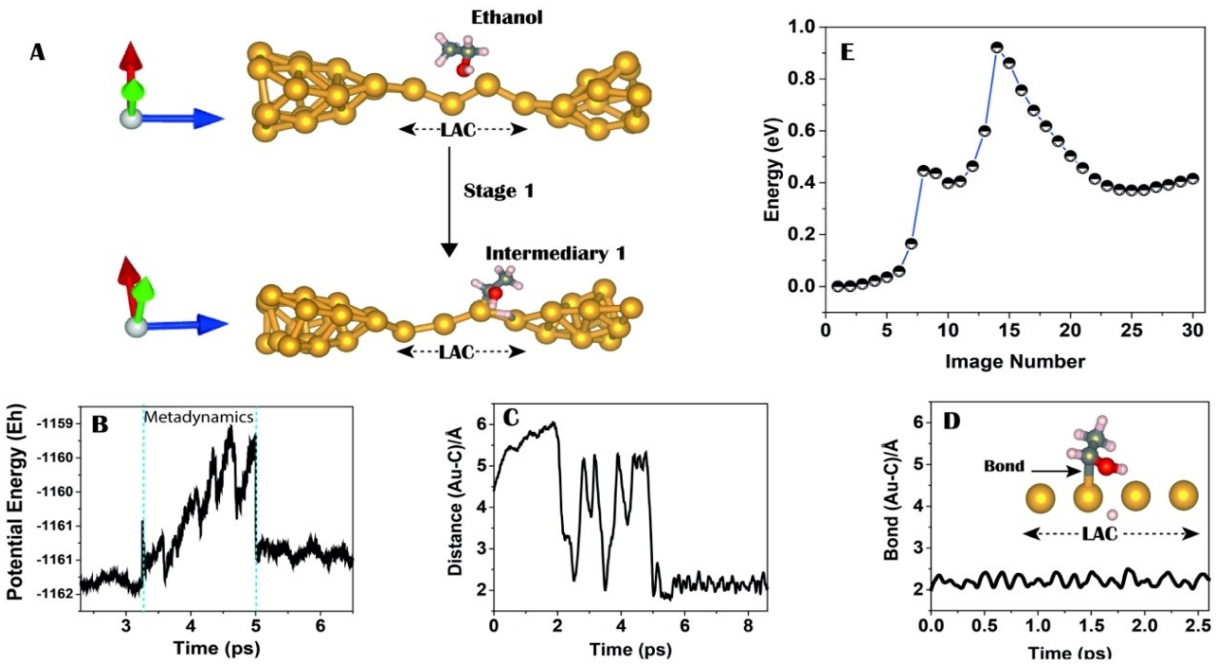

Figure 5. Chemical reaction of ethanol supported on Au–NW with LAC without the presence of impurity. (A) Graphical representation of the chemical reaction showing the reagent and the product (In this step, the product is the intermediate in the overall ethanol oxidation reaction). (B) Behavior of the system's potential energy before, during, and after applying metadynamics. (C) Behavior of the Au–C distance throughout the simulation. The Au–C distance is used to obtain information on the formation and stability of the intermediary. (D) Stability of the intermediate formed, measured indirectly using the Au–C bond during a 2.5 ps trajectory simulation. (E) NEB of the minimum energy path for the chemical reaction of ethanol in its first stage.

diary. In this case, the trajectory was extended for approximately 2.5 ps (Figure 5D). It is observed that the intermediate remains stable along the simulation path, keeping its Au–C bond fluctuating at approximately 2.1 Å. Therefore, with these results, it can be stated that ethanol reaction will occur in stages and will involve at least the formation of an intermediate that will be stabilized in LAC (Figure 5D).

Regarding the minimum energy path of the chemical reaction, the NEB results show two interesting things (Figure 5E): (i) The activation energy barrier turned out to be ~0.96 eV, which implies overcoming a height of 37 times the height defined by a thermal fluctuation at 300 K (K_BT = 25.7 meV), to observe a chemical reaction. This suggests that the formation of an intermediate (in pure NW) requires a relatively high activation energy barrier. (ii) The formation of the intermediary takes place in an endothermic chemical reaction. Therefore, to favor the reaction kinetically, an increase in the temperature of the system would be necessary. Also, it is expected that in the next stage of the reaction, the reaction product should be formed in an exothermic process.

The second stage of the chemical reaction could lead to the formation of acetaldehyde (C_2H_4O). Its formation is plausible, as it has been observed experimentally in different works.[64–66] Therefore, assuming that the second step of the reaction forms acetaldehyde, then, in this case, only the proton of intermediary-1 (–O**H**) should be freed from its structure by proton transfer (Figure 5 A, intermediary-1). The NEB results show that an activation energy barrier of ~0.36 eV has to be overcome for proton transfer to a LAC gold atom to occur (Figure S7). This energy barrier turned out to be much smaller than the energy barrier crossed in the first stage (~0.96 eV). It is more likely that this energy barrier is overcome by thermal fluctuations more easily than the barrier of the first stage since it only represents 14 times the barrier height defined by a thermal fluctuation at room temperature. In any case, the reaction could occur at room temperature since the energy barrier is not excessively high. The NEB results also show that the formation of acetaldehyde takes place in an endothermic process. Therefore, the formation of acetaldehyde from ethanol (in pure LAC) is a purely endothermic process where an increase in temperature could be adequate to easily overcome, mainly, the barrier of the first stage.

Experimental studies show that the dehydrogenation of ethanol occurs at temperatures around 260 °C. For example, specifically on pure copper surfaces, this reaction occurs at temperatures around 260–290 °C.[67] Therefore, our result suggests that within the experimentally observed temperature range, the proposed reaction mechanism occurs easily.

On the other hand, transferring the proton to the LAC would be much more accessible (much lower activation energy barrier) if the LAC had an impurity (oxygen) in its structure since a proton transfer from one oxygen to another is far more favorable. It could even lower the activation barrier of the first stage. Therefore, it might be advantageous to add oxygen impurity in the LAC. With that in mind, to form acetaldehyde in the next step of the chemical reaction, we considered the case of an oxygen impurity atom in the LAC.

LAC with an Oxygen Impurity

In this part, the study begins with the presence of an oxygen impurity in the LAC structure (Figure 6 A). The simulations show the same results observed in the previous case (pure LAC). That

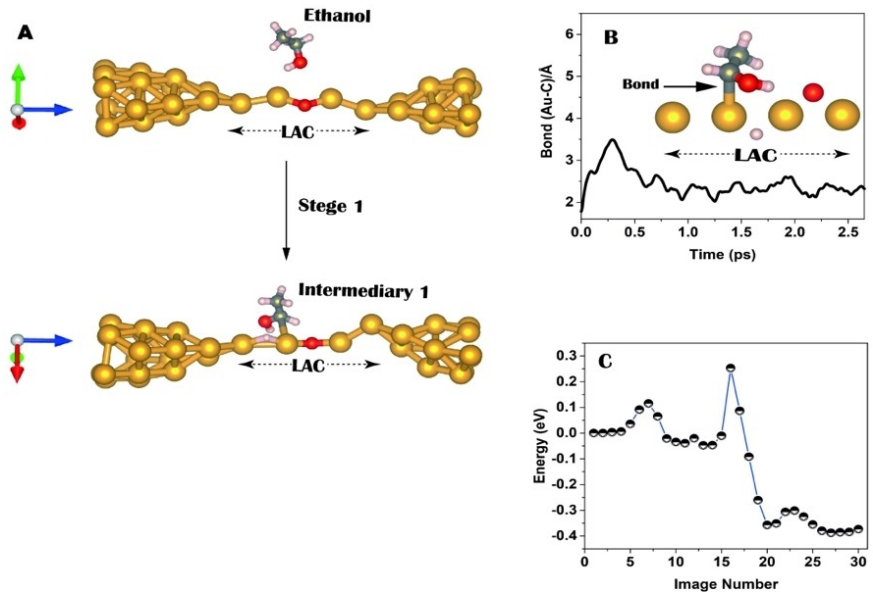

Figure 6. Initial step of the chemical reaction of ethanol supported on Au–NW with LAC containing an oxygen atom impurity in its structure. (A) Graphical representation of a chemical reaction, where the reactant and the product are shown (In this step, the product is the intermediate in the overall ethanol oxidation reaction). (B) Behavior of the intermediary-1 Au–C bond during a 2.5 ps trajectory simulation. (C) NEB of the minimum energy path for the chemical reaction of ethanol in its first stage.

is, the formation of the same intermediary-1 as in the first step is observed (Figure 5 A). Where, again, activation at the β-C–H bond cleavage is achieved. Additionally, it is observed that intermediary-1 maintains its stability over time (Figure 6 B). That is, the Au–C bond remains fluctuating around 2.2 Å. Also, complementarily, the interaction of H that was directed towards the LAC is described in the supplementary material (Figure S8).

Furthermore, it is observed that one of the main differences in relation to pure LAC is the kinetic behavior in the formation of intermediate-1 (Figure 6 C).

The NEB results showed that the activation energy barrier strongly decreases relative to the chemical reaction barrier in pure LAC (Figure 5E). In this case, a much smaller activation energy barrier of ~0.30 eV was found (Figure 6C). That is, now, the height of the barrier becomes only 11 times the height defined by the thermal fluctuation at room temperature, and no longer 37 times as observed in the pure LAC. This shows that the presence of oxygen (in LAC) modifies the reaction kinetics, favoring the formation of intermediary-1. A behavior with these characteristics was expected since the ELF results (presented above) showed a different chemical nature between LACs with and without impurity. Furthermore, another difference found is that the local minimum established by the formation of intermediary-1 is more stable than the local minimum defined by the reagent. That is, in the presence of oxygen, the formation of intermediary-1 takes place in an exothermic process. Therefore, highlighting the role of oxygen, it can be said that oxygen, in addition to strengthening the chemical bond of the LAC, also controls the kinetics of the first step of a chemical reaction (chemical reaction acceleration), and forms a more stable intermediate-1.

Experimental studies showed that, in the presence of oxygen, less temperature is required to form acetaldehyde. For example, using molecular beam scattering ultra-high vacuum (UHV), on the surface of PdAu,[111] traces of acetaldehyde were observed around 200 K.[68] Also, the theoretically calculated activation energy barrier for acetaldehyde formation (for different reaction mechanisms) varies between 0.4–2.0 eV.[68] Another theoretical study showed that, on an Au[111] gold surface in the presence of oxygen, the barrier needed to activate the β-C–H bond is ~0.29 eV.[69] Other studies, in the presence of oxygen, also showed similar activation energy barriers.[70–73] This shows that our result is in agreement with works similar to ours.

Next, we explored the role of oxygen in the following stage of the reaction, that is, in the formation of acetaldehyde (Figure 7A). At this step, acetaldehyde formation requires proton transfer from intermediary-1 (–O**H**) to the LAC. Therefore, we consider only the H–O transfer (Figure 7A). For this, molecular dynamics (without metadynamics) was used to observe the **H**–**O** transfer. Intermediary-1 maintains its stability, while its –O**H** group is relatively far from the oxygen atom of the LAC (H–O distance). This can be seen in the temporal evolution of the Au–C and O–H distances (Figure 7B and C). It is also observed that while the O–H distance decreases, the intermediary destabilizes (increasing the Au–C distance) to form acetaldehyde.

In the process of acetaldehyde formation (which implies only the transfer of a proton), it is observed that the potential energy of the system abruptly decreases to a more negative

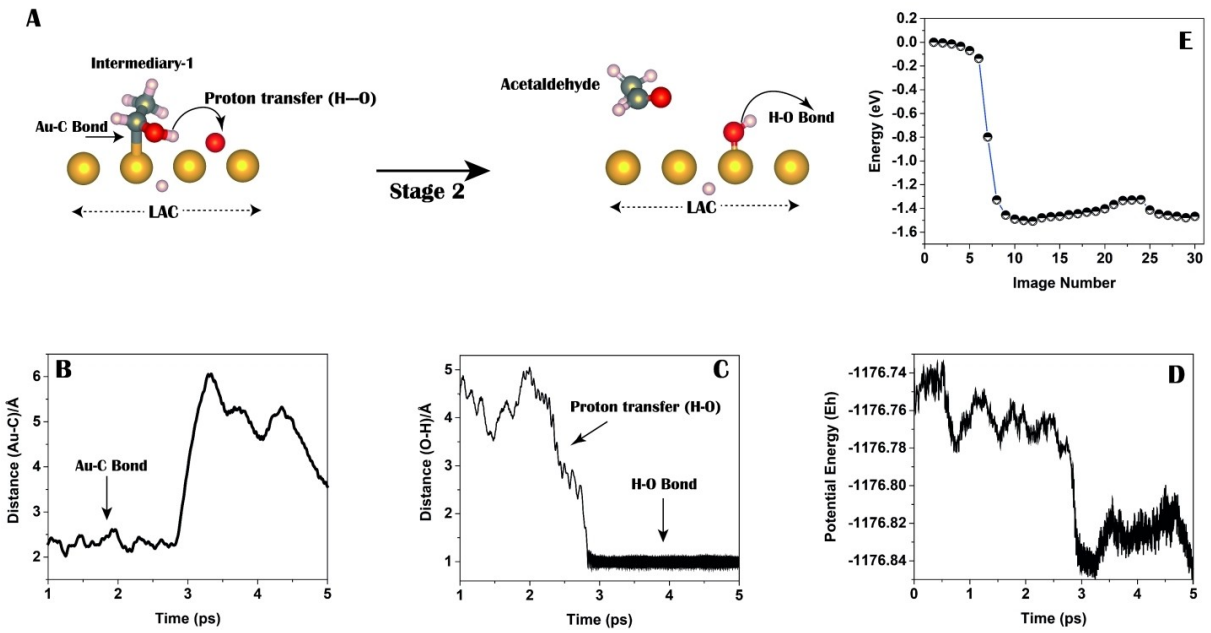

Figure 7. Final step of the chemical reaction of ethanol supported on Au–NW with LAC containing impurity in its structure (an oxygen atom). (A) Representation of the chemical reaction showing the reactant (intermediary) and product (acetaldehyde), this is an idealized graphical representation of the chemical reaction showing the reagent and product, considering only the LAC part of the NW to achieve a better visualization. (B) and (C) These plots detail the time evolution of Au–C and O–H bonds over approximately 5 ps. (D) Potential energy behavior of the system focused on the formation of acetaldehyde. (E) NEB of the minimum energy pathway for acetaldehyde formation from the intermediary.

value (Figure 7D), suggesting that the local minimum defined by the formation of the product (acetaldehyde) is still more stable than the other local minimum defined by the intermediate and ethanol. The NEB result confirms that acetaldehyde formation effectively leads to a much more stable local minimum (Figure 7E). NEB analysis (Figure 7E) also shows that proton transfer occurs at negligible energy cost (~0.01 eV). That is, it is only necessary that the –O**H** and oxygen groups in the LAC (H–Au) be relatively close. Therefore, this suggests that intermediary-1 will lose stability as the presence of impurities (oxygen) in LAC increases.

With the presence of an oxygen impurity in the LAC, the formation of another intermediary was also observed. In this case, from intermediary-1 (Figure 8, P1), the formation of intermediary-2 (Figure 8, P2) was also seen. Instead of a direct proton transfer to form acetaldehyde, the carbon atom that is bonded to the gold atom first prefers to bond to the oxygen of LAC (Figure 8, intermediary-2). The NEB result shows that once intermediary-2 is formed, the energy cost to return to intermediary-1 is quite high (~2.5 eV). Therefore, once intermediary-2 is formed, the reaction route to form acetaldehyde takes another path (Figure 8, P2, P3, P4, and P5).

NEB also shows that once intermediary-2 is formed, the energy cost to form acetaldehyde is relatively low (Figure 8, energy difference between P3 and P2 ~0.6 eV). This process involves intramolecular proton transfer synchronized with a C–O bond breaking (Figure 8, P3). The size of the energy barrier is affordable to allow the reaction by thermal fluctuations at ambient temperature (300 K). Therefore, intermediary-2 also leads to the formation of acetaldehyde. At this stage of our analysis, we could say that ethanol oxidation, supported in NW with an oxygen impurity, could occur via two reaction pathways (Figure 9). Out of these two possibilities, the pathway involving the formation of only intermediary-1 (Figure 7) is a little more favored for presenting a lower energy barrier to form acetaldehyde.

Conclusions

In this work, different techniques were used to explore the chemical behavior of NWs in order to study the reactions that occur when ethanol interacts with Au–NWs LACs containing an oxygen impurity in its structure and also in its pure form.

Electrostatic molecular potential, electron density difference and electron localization function techniques showed interesting results. It is concluded that the most reactive part of the gold nanowires is in its linear atomic chain (LAC). LACs with and

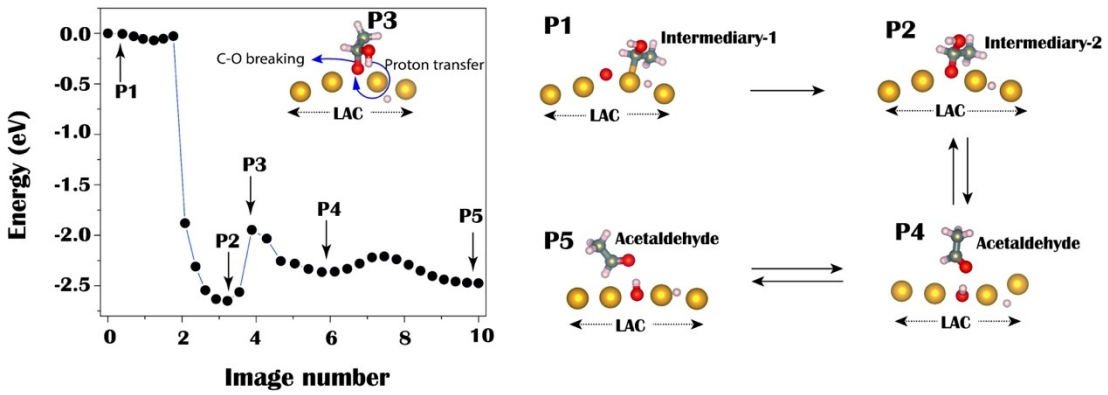

Figure 8. NEB results of the minimum energy path of the events leading to the formation of Intermediary-2 from Intermediary-1. The formation of acetaldehyde from the intermediate is also shown. The graph was taken from the simulation trajectory, considering only the LAC part of the NW to achieve a better visualization.

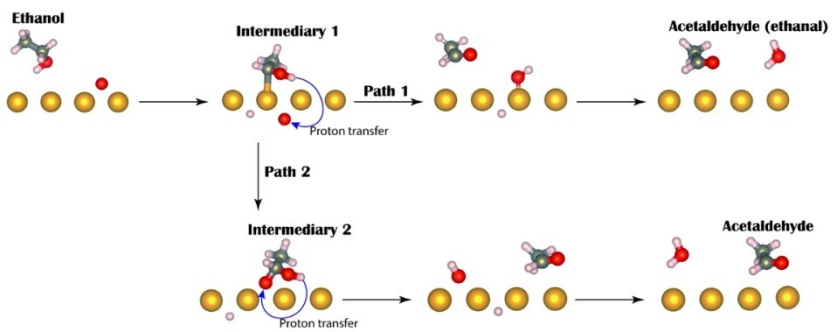

Figure 9. Idealized graphical representation of the reaction pathways observed in the formation of acetaldehyde, only the LAC part of the NW is represented for a better visualization. Intermediary-1 can directly leads to acetaldehyde formation. Additionally, intermediary-1 can form another intermediary-2, which also leads to the formation of acetaldehyde.

without oxygen impurity in their structure are sensitive to interactions with ethanol, drastically modifying their nucleophilic character. Furthermore, it was found that the oxygen impurity plays different roles in the behavior of the NW. It acts as an anchor for the gold atoms, providing stability to the LAC, and also lowers the activation energy barriers, facilitating the chemical reactions of ethanol.

Ab initio molecular dynamics simulations showed that the chemical reaction of ethanol has a different kinetic and thermodynamic behavior when they occur in NWs with and without oxygen impurity.

Regarding the kinetic behavior, in the first stage of the ethanol reaction, the activation energy barrier is reduced by ~69% when the reaction occurs in the LAC with oxygen impurity. Regarding thermodynamic behavior, the formation of intermediary-1 occurs in an exothermic process when the LAC contains oxygen impurity, and in an endothermic process when the LAC is pure.

It was also observed that, when the reaction occurs in the LAC with oxygen impurity, the ethanol reaction leads to the formation of acetaldehyde through two different reaction pathways. Therefore, one important conclusion of the present work is that the presence of the O impurity in the LAC is of paramount importance to the enhanced reactivity of the Au nanowire.

Supporting Information Summary

Additional information on optimization of geometry, alternative methodology DFT, ELF and EDD analysis, adsorption energy, bond energy, PES and NEB analysis.

Additional cited references within the supporting information are the references 74,75 and 76.

Acknowledgements

This work was carried out with the support of the São Paulo Research Foundation – FAPESP (Grant: 2013/07296-2, 2016/23891-6, 2017/26105-4 and 2020/11815-9, projects). Simulations performed at CCJDR-UNICAMP, Simulations performed at Centro de Computação John David Rogers, CCJDR-IFGW-UNICAMP.

Conflict of Interest

The authors declare no conflict of interest.

Data Availability Statement

The data that support the findings of this study are available from the corresponding author upon reasonable request.

Keywords: density functional calculations · ethanol oxidation · gold nanowire · molecular dynamics · linear atomic chain

[1] Y. C. Kim, S. Y. Kim, *RSC Adv.* **2018**, *8*, 19532–19538.
[2] A. Saj, S. Alketbi, S. M. Ansari, D. H. Anjum, B. Mohammad, H. M. Aldosari, *Nanomaterials* **2022**, *12*, 763.
[3] J. Tang, D. Tsoukalas, *J. Nano R.* **2009**, *6*, 67–74.
[4] A. H. Tanzil, S. T. Sultana, S. R. Saunders, A. C. Dohnalkova, L. Shi, E. Davenport, P. Ha, H. Beyenal, *Enzyme Microb. Technol.* **2016**, *95*, 69–75.
[5] Y.-C. Yeh, B. Creran, V. M. Rotello, *Nanoscale* **2012**, *4*, 1871–1880.
[6] R. Zhang, M. Hummelgård, H. Olin, *PLoS One* **2012**, *7*, e30469.
[7] E. Z. da Silva, A. J. R. da Silva, A. Fazzio, *Phys. Rev. Lett.* **2001**, *87*, 256102.
[8] T. Kizuka, *Phys. Rev. B* **2008**, *77*, 155401.
[9] H. Ohnishi, Y. Kondo, K. Takayanagi, *Nature* **1998**, *395*, 780–783.
[10] V. Rodrigues, D. Ugarte, *Phys. Rev. B* **2001**, *63*, 073405.
[11] W. H. A. Thijssen, D. Marjenburgh, R. H. Bremmer, J. M. van Ruitenbeek, *Phys. Rev. Lett.* **2006**, *96*, 026806.
[12] U. Landman, W. D. Luedtke, B. E. Salisbury, R. L. Whetten, *Phys. Rev. Lett.* **1996**, *77*, 1362–1365.
[13] S. B. Legoas, D. S. Galvão, V. Rodrigues, D. Ugarte, *Phys. Rev. Lett.* **2002**, *88*, 076105.
[14] F. D. Novaes, A. J. R. da Silva, E. Z. da Silva, A. Fazzio, *Phys. Rev. Lett.* **2003**, *90*, 036101.
[15] F. D. Novaes, A. J. R. da Silva, E. Z. da Silva, A. Fazzio, *Phys. Rev. Lett.* **2006**, *96*, 016104.
[16] A. P. F. Nascimento, M. A. San-Miguel, E. Z. da Silva, *Phys. Rev. B* **2014**, *89*, 085417.
[17] G. Li, R. Jin, *Acc. Chem. Res.* **2013**, *46*, 1749–1758.
[18] H. Seong, V. Efremov, G. Park, H. Kim, J. S. Yoo, D. Lee, *Angew. Chem. Int. Ed.* **2021**, *60*, 14563–14570.
[19] H. Xu, D. Cheng, Y. Gao, X. C. Zeng, *ACS Catal.* **2018**, *8*, 9702–9710.
[20] Y. Zhao, S. Zhuang, L. Liao, C. Wang, N. Xia, Z. Gan, W. Gu, J. Li, H. Deng, Z. Wu, *J. Am. Chem. Soc.* **2020**, *142*, 973–977.
[21] Y. Zhu, H. Qian, R. Jin, *J. Mater. Chem.* **2011**, *21*, 6793–6799.
[22] P. V. Martin, E. Zoloff Michoff, S. A. Dassie, E. P. M. Leiva, *Electrodeposited Nanowires and Their Applications*, ed. N. Lupu, Romania, **2010**, vol. 1, ch. 2, p. 236.
[23] A. S. Goldman, K. I. Goldberg, *J. Am. Chem. Soc.* **2004**, *885(1)*, 1–43.
[24] P. Lu, T. C. Boorman, A. M. Z. Slawin, I. Larrosa, *J. Am. Chem. Soc.* **2010**, *132*, 5580–5581.
[25] B. Ma, L. Liu, J. Zhang, *Asian J. Org. Chem.* **2018**, *7*, 2015–2025.
[26] C. Sivaraj, A. Ramkumar, N. Sankaran, T. Gandhi, *Org. Biomol. Chem.* **2021**, *19*, 8165–8183.
[27] J. Hutter, M. Iannuzzi, F. Schiffmann, J. Vande Vondele, *WIREs Comput. Mol. Sci.* **2014**, *4*, 15–25.
[28] T. D. Kühne, M. Iannuzzi, M. D. Ben, V. V. Rybkin, P. Seewald, F. Stein, T. Laino, R. Z. Khaliullin, O. Schütt, F. Schiffmann, D. Golze, J. Wilhelm, S. Chulkov, M. H. Bani-Hashemian, V. Weber, U. Borštnik, M. Taillefumier, A. S. Jakobovits, A. Lazzaro, H. Pabst, T. Müller, R. Schade, M. Guidon, S. Andermatt, N. Holmberg, G. K. Schenter, A. Hehn, A. Bussy, F. Belleflamme, G. Tabacchi, A. Glöß, M. Lass, I. Bethune, C. J. Mundy, C. Plessl, M. Watkins, J. Vande Vondele, M. Krack, J. Hutter, *J. Chem. Phys.* **2020**, *152*, 194103.
[29] J. Vande Vondele, M. Krack, F. Mohamed, M. Parrinello, T. Chassaing, J. Hutter, *Comput. Phys. Commun.* **2005**, *167*, 103–128.
[30] G. Lippert, J. Hutter, M. Parrinello, *Mol. Phys.* **1997**, *92*, 477–488.
[31] J. Vande Vondele, J. Hutter, *J. Chem. Phys.* **2003**, *118*, 4365–4369.
[32] M. Ernzerhof, G. E. Scuseria, *J. Chem. Phys.* **1999**, *110*, 5029–5036.
[33] L. S. Pedroza, A. J. R. da Silva, K. Capelle, *Phys. Rev. B* **2009**, *79*, 201106.
[34] S. Grimme, J. Antony, S. Ehrlich, H. Krieg, *J. Chem. Phys.* **2010**, *132*, 154104.
[35] S. Grimme, S. Ehrlich, L. Goerigk, *J. Comput. Chem.* **2011**, *32*, 1456–1465.
[36] D. G. A. Smith, L. A. Burns, K. Patkowski, C. D. Sherrill, *J. Phys. Chem. Lett.* **2016**, *7*, 2197–2203.
[37] J. Vande Vondele, J. Hutter, *J. Chem. Phys.* **2007**, *127*, 114105.
[38] S. Goedecker, M. Teter, J. Hutter, *Phys. Rev. B* **1996**, *54*, 1703–1710.
[39] C. Hartwigsen, S. Goedecker, J. Hutter, *Phys. Rev. B* **1998**, *58*, 3641–3662.
[40] A. Kovács, J. Cz. Dobrowolski, S. Ostrowski, J. E. Rode, *Int. J. Quantum Chem.* **2017**, *117*, e25358.
[41] S. Tsuzuki, T. Uchimaru, *Phys. Chem. Chem. Phys.* **2020**, *22*, 22508–22519.
[42] L. Goerigk, A. Hansen, C. Bauer, S. Ehrlich, A. Najibi, S. Grimme, *Phys. Chem. Chem. Phys.* **2017**, *19*, 32184–32215.

[43] Y.-S. Lin, G.-D. Li, S.-P. Mao, J.-D. Chai, *J. Chem. Theory Comput.* **2013**, *9*, 263–272.
[44] D. Cortés-Arriagada, M. P. Oyarzún, L. Sanhueza, A. Toro-Labbé, *J. Phys. Chem. A* **2015**, *119*, 6909–6918.
[45] P. J. Hay, W. R. Wadt, *J. Chem. Phys.* **1985**, *82*, 299–310.
[46] L. E. Roy, P. J. Hay, R. L. Martin, *J. Chem. Theory Comput.* **2008**, *4*, 1029–1031.
[47] G. J. Martyna, M. L. Klein, M. Tuckerman, *J. Chem. Phys.* **1992**, *97*, 2635–2643.
[48] S. Nosé, *J. Chem. Phys.* **1984**, *81*, 511–519.
[49] P. K. Patra, B. Bhattacharya, *Phys. Rev. E* **2014**, *90*, 043304.
[50] A. Barducci, M. Bonomi, M. Parrinello, *Comput. Mol. Sci.* **2011**, *1*, 826–843.
[51] M. Iannuzzi, A. Laio, M. Parrinello, *Phys. Rev. Lett.* **2003**, *90*, 238302.
[52] G. Henkelman, H. Jónsson, *J. Chem. Phys.* **2000**, *113*, 9978–9985.
[53] G. Henkelman, B. P. Uberuaga, H. Jónsson, *J. Chem. Phys.* **2000**, *113*, 9901–9904.
[54] M. Weiß, M. Brehm, *Molecules* **2020**, *25*, 5861.
[55] K. Koumpouras, J. A. Larsson, *J. Phys. Condens. Matter* **2020**, *32*, 315502.
[56] B. Silvi, C. Gatti, *J. Phys. Chem. A* **2000**, *104*, 947–953.
[57] J. S. Murray, P. Politzer, *WIREs Comput. Mol. Sci.* **2011**, *1*, 153–163.
[58] J. Gasteiger, X. Li, C. Rudolph, J. Sadowski, J. Zupan, *J. Am. Chem. Soc.* **1994**, *116*, 4608–4620.
[59] M. A. San-Miguel, E. P. M. Amorim, E. Z. da Silva, *J. Phys. Chem. C* **2015**, *119*, 2456–2461.
[60] B. F. Zornio, E. Z. da Silva, M. A. San-Miguel, *Theor. Chem. Acc.* **2017**, *136*, 63.
[61] J. Fallaque-Najar, J.-C. Morales-Gomero, V. Timon, *Surf. Sci.* **2019**, *689*, 121458.
[62] R. L. H. Freire, A. Kiejna, J. L. F. Da Silva, *Phys. Chem. Chem. Phys.* **2016**, *18*, 29526–29536.
[63] J. Gong, C. B. Mullins, *J. Am. Chem. Soc.* **2008**, *130*, 16458–16459.
[64] P. Liu, E. J. M. Hensen, *J. Am. Chem. Soc.* **2013**, *135*, 14032–14035.
[65] X. Liu, B. Xu, J. Haubrich, R. J. Madix, C. M. Friend, *J. Am. Chem. Soc.* **2009**, *131*, 5757–5759.
[66] S. Mostrou, A. Nagl, M. Ranocchiari, K. Föttinger, J. A. van Bokhoven, *Chem. Commun.* **2019**, *55*, 11833–11836.
[67] M. Eckert, G. Fleischmann, R. Jira, H. M. Bolt, K. Golka, Acetaldehyde, in *Ullmann's Encyclopedia of Industrial Chemistry*, Wiley-VCH Verlag GmbH & Co. KGaA, **2006**, p. 192–207.
[68] E. J. Evans, H. Li, S. Han, G. Henkelman, C. B. Mullins, *ACS Catal.* **2019**, *9*, 4516–4525.
[69] Q. Meng, Y. Shen, J. Xu, J. Gong, *Chin. J. Catal.* **2012**, *33*, 407–415.
[70] H. Li, G. Henkelman, *J. Phys. Chem. C* **2017**, *121*, 27504–27510.
[71] E. J. Evans, H. Li, W.-Y. Yu, G. M. Mullen, G. Henkelman, C. B. Mullins, *Phys. Chem. Chem. Phys.* **2017**, *19*, 30578–30589.
[72] Z.-F. Xu, Y. Wang, *J. Phys. Chem. C* **2011**, *115*, 20565–20571.
[73] D. Zanchet, J. B. O. Santos, S. Damyanova, J. M. R. Gallo, J. M. C. Bueno, *ACS Catal.* **2015**, *5*, 3841–3863.
[74] L. You-Sheng, Guan-De Li, Shan-Ping Mao, Jeng-Da Chai, *J. Chem. Theory Comput.* **2013**, *9*, 263–272.
[75] X. Xuefei, D. G. Truhlar, *J. Chem. Theory Comput.* **2011**, *7*, 2766–2779.
[76] M. Satoshi, Y. Harabuchi, Y. Ono, T. Taketsugu, K. Morokuma, *Int. J. Quantum Chem.* **2015**, *115*, 258–269.

Manuscript received: September 29, 2022
Revised manuscript received: November 14, 2022
Accepted manuscript online: November 23, 2022
Version of record online: December 13, 2022